# Atomic and Molecular Adsorption on Ir(111)

**William P. Krekelberg, Jeff Greeley, and Manos Mavrikakis***

*Department of Chemical and Biological Engineering, University of Wisconsin−Madison, Madison, Wisconsin 53706-1691*

*Received: June 23, 2003; In Final Form: October 22, 2003*

The chemisorption of atomic (H, O, N, S, C), molecular ($N_2$, CO, NO, $NH_3$), and radical ($CH_3$, OH, NOH) species on Ir(111) has been systematically studied. Self-consistent, periodic, density functional theory (DFT-GGA) calculations, using PW91 and RPBE functionals, have been used to determine preferred binding sites, chemisorbed structures, binding energies, vibrational frequencies, and the effect of surface relaxation for the above species at 0.25 ML surface coverage. The following order in binding energies from least to most strongly bound was determined: $N_2 < NH_3 < NO < CH_3 < CO < OH < H < NOH < O < N < S < C$. A preference for 3-fold sites for the atomic adsorbates was observed, with the exception of atomic H, which prefers top sites. Molecular species showed a preference for top sites with the exception of NOH; this species preferred fcc sites. Surface relaxation had only a small effect on energetics in most cases. Calculated vibrational frequencies, in general, were in good agreement with experimental frequencies and support experimentally proposed site preferences for all adsorbates where data are available. Finally, the thermochemistry of CO, NO, NOH, $N_2$, $NH_3$, and $CH_3$ decomposition on Ir(111) was examined, leading to predictions for each species of the preference for either desorption or decomposition.

## 1. Introduction

Iridium, much like other late transition metals, shows a wide variety of potential applications as a heterogeneous catalyst in the chemical industry. In alkanes, Ir and Ir-alloy catalysts are used in reactions that require the activation of C−H bonds.[1] Several reactions of industrial significance have this requirement, including the conversion of saturated hydrocarbons in petroleum naphtha fractions to aromatic compounds (dehydrocyclization of alkanes and dehydrogenation of cycloalkanes) which are high-octane components of gasoline,[2] the conversion of lower alkanes to feedstock chemicals, and the steam reforming of methane as well as the conversion of methane to higher hydrocarbons or methanol.[3,4] In addition, iridium is a potential catalyst for the $CO_x$-free production of hydrogen from ammonia.[5] Further, iridium is being considered for the improvement of the automobile catalytic converter because of its ability to decompose NO[6] and to reduce $NO_x$ with hydrocarbons.[7] Finally, two homogeneous iridium-based catalysts have demonstrated additional uses for this metal. One has improved the production of acetic acid by a methanol carbonylation process,[8] and the other catalyzes the liquid-phase dehydrogenation of cycloalkanes; this process could produce hydrogen gas from gasoline to be used in fuel cells.[9]

The desire to gain an understanding of the above processes has motivated much fundamental research on single-crystal iridium. The interactions between *atomic species* and single-crystal iridium surfaces have been the subject of several research studies. Adsorbed oxygen atoms on Ir(111) have been investigated with low-energy electron diffraction (LEED),[10−13] UV photoelectron spectroscopy (UPS),[10] and X-ray photoelectron spectroscopy (XPS).[14,15] Atomic nitrogen overlayer structures on the Ir(110) surface have been studied with LEED.[16] The overlayer structure of sulfur on the Ir(111) surface has been investigated with LEED.[17] Dissociative chemisorption of hydrogen on Ir(111) has been studied with high-resolution electron energy loss spectroscopy (HREELS).[18] Finally, the coadsoption of hydrogen and potassium on Ir(111) has been studied with Auger electron spectroscopy and LEED.[19]

There have been an even larger number of studies of adsorption of *molecular species* on iridium. Dinitrogen ($N_2$) adsorption on Ir(111) has been studied with EELS and temperature-programmed desorption (TPD).[6] Nitric oxide adsorption on iridium has been investigated with EELS, TPD, supersonic molecular beam techniques, and DFT calculations.[6,20,21] The adsorption of carbon monoxide on Ir(111) has been investigated in great detail. Fourier transformed infrared reflection−adsorption spectroscopy (FT-IRAS), TPD, HREELS, XPS, UPS, and LEED have been used to determine adsorption site preferences at several coverages.[13,22−24] The coadsorption of CO and hydrogen on Ir(111) has been investigated with TPD and IRAS,[25] and the effect of preadsorbed oxygen on CO adsorption was studied with molecular beam spectroscopy.[26] FT-IRAS was used to analyze the adsorption of CO on Ir(111) at several surface coverages.[22] The chemisorption of the methyl radical has been investigated with DFT in connection with the decomposition of methane on Ir(111).[27] Lastly, the adsorbed structure of ammonia on Ir(111)[28] was investigated with angle-resolved photoemission experiments.

Much experimental research has been conducted to gain understanding of the *kinetics* of adsorption, desorption, and reactions on iridium surfaces. Ammonia decomposition on Ir-(100) has been studied with TPD experiments,[29] and ammonia oxidation on Ir(110) has been investigated with LEED.[30] Molecular beam titration has been employed to analyze the oxidation of CO on Ir(110).[31] Association and dissociation kinetics have also been investigated for CO over Ir(111) with

* To whom correspondence should be addressed. E-mail: manos@engr.wisc.edu. Phone: (608) 262-9053. Fax: (608) 262-5434.

10.1021/jp035786c CCC: $27.50 
Published on Web 12/18/2003

LEED, FT-IRAS,[25,32,33] and DFT.[34] On Ir(111), the adsorption of NO has been studied with EELS,[20] and the dissociation of NO has been analyzed with TPD and EELS.[6] The presence of the intermediate NOH has been hypothesized to exist in the reduction of NO in the presence of $H_2$ or alkanes, though this species has been difficult to isolate experimentally.[35]

Computational analysis,[36] coupled with the above studies, can give insight to the fundamental surface science of Ir(111). Similar to our previous work on Rh(111),[37] we present here a systematic study of the chemisorption structure and energetics of several atomic (H, O, N, S, C), molecular ($N_2$, CO, NO, $NH_3$), and radical ($CH_3$, OH, NOH) species on the Ir(111) surface. Periodic, self-consistent DFT calculations are used to determine preferred binding sites and binding energies for the adsorbed species. Diffusion barriers and vibrational modes are determined. Finally, the thermochemistry of CO, NO, $N_2$, NOH, $NH_3$, and $CH_3$ dissociation on Ir(111) is examined.

## 2. Methods

All calculations are carried out with DACAPO.[38] A four-layer slab of iridium, periodically repeated in a super cell geometry with five equivalent layers of vacuum between any two successive metal slabs, is used. A $2\times2$ unit cell, corresponding to a surface coverage of 0.25 ML, is used. Adsorption is allowed on only one of the two exposed surfaces, and the electrostatic potential is adjusted accordingly.[39] Initial computations are performed with metal atoms fixed in their bulk-truncated positions. The calculations are then repeated for all adsorbate geometries allowing the top two metal layers to relax. Ionic cores are described by ultrasoft pseudopotentials,[40] and the Kohn−Sham one-electron valence states are expanded in a basis of plane waves with a kinetic energy cutoff of 25 Ry. The surface Brillouin zone is sampled at 18 special k points. In all cases, convergence with respect to the k point set and with respect to the number of metal layers included is confirmed. The exchange-correlation energy and potential are described by two generalized gradient approximations, self-consistently with GGA-PW91[41,42] and non-self-consistently with RPBE.[38] The self-consistent PW91 density is determined by iterative diagonalization of the Kohn−Sham hamiltonian, Fermi population of the Kohn−Sham states ($k_BT = 0.1$ eV), and Pulay mixing of the resulting electronic density.[43] All total energies have been extrapolated to $k_BT = 0$ eV. The calculated lattice constant for bulk iridium, 3.86 Å (PW91), is within 0.5% of the experimental value of 3.84 Å.[44] Vibrational frequencies are determined from diagonalization of the mass-weighted Hessian matrix; a second-order finite difference approximation of the PW91-calculated force derivatives is used to construct this matrix.[45]

For gas-phase calculations, large unit cells (approximately 7 Å on a side) were used to minimize spurious interactions between periodic images, and care was taken to ensure that the correct, spin-polarized orbital occupations were obtained for each species. PW91 [RPBE] gas-phase bond energies for OH, CO, NO, and $N_2$ (in eV) are 4.61 [4.53], 10.96 [10.59], 6.74 [6.50], and 9.63 [9.47], respectively. The corresponding experimental results for these quantities (in eV) are 4.44, 11.17, 6.55, and 9.80.[46] PW91 [RPBE] energy changes for $NH_3$ to N + 3H, and $CH_3$ to C + 3H (in eV) are 12.75 [12.50] and 13.40 [13.16], respectively, and the corresponding experimental values are 12.17 and 12.71 eV.[46]

## 3. Results and Discussion

This section contains a description of the chemisorption properties for all the adsorbates studied, including binding energies, diffusion barrier estimates, site preferences, the effect of surface relaxation, and vibrational frequencies. Binding energies are presented for both PW91 and RPBE functionals with the latter given in square brackets. The effects of surface relaxation and coordination preferences are discussed. For atomic, molecular, and radical adsorbates, a summary of the calculated binding energies for fixed and relaxed surfaces, together with estimates for the diffusion barriers, are given (Figures 1 and 2). The thermochemistry of the adsorption and decomposition of CO, NO, NOH, $N_2$, $NH_3$, and $CH_3$ is then presented.

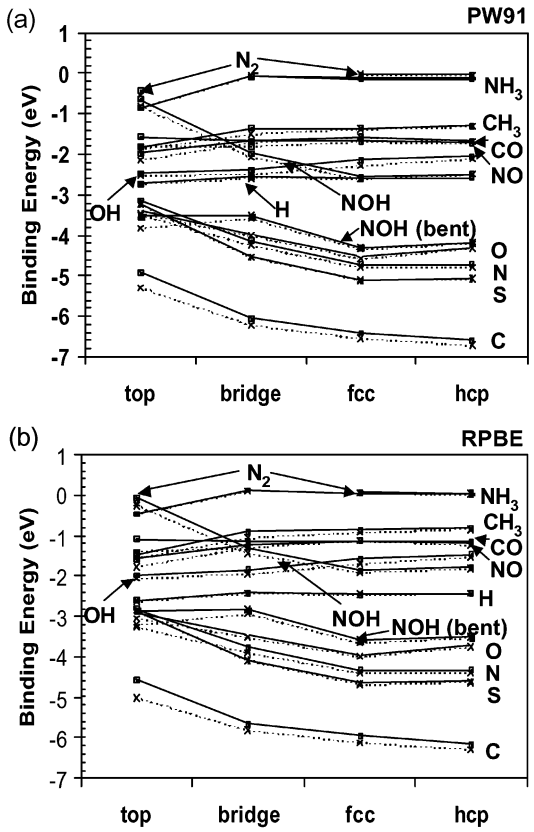


**Figure 1.** Binding energies of atomic, molecular, and radical adsorbates on Ir(111), calculated with the (a) PW91 and (b) RPBE functionals (solid line, fixed surface; dashed line, relaxed surface). Reference zero corresponds to gas-phase species at infinite separation from the surface. Lines are guides to the eye only.

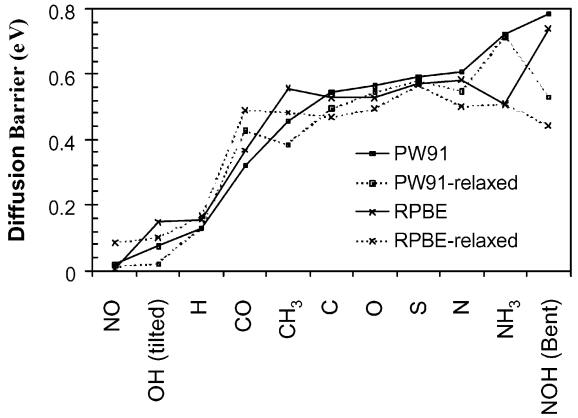


**Figure 2.** Estimates for diffusion barriers on Ir(111). The adsorbates are ordered from lowest to highest diffusion barrier. Lines are guides to the eye only.

**Adsorption of Atoms.** Atomic *hydrogen* is the least strongly bound of the atomic adsorbates studied on Ir(111), with a

**TABLE 1: Calculated Binding Energies and Calculated and Experimental Vibrational Frequencies of Atomic Adsorbates on a *Relaxed* Ir(111) Surface at 0.25 ML Coverage[a]**

| | best site | | binding energy (eV) PW91 [RPBE] | | | | $\nu$ (cm$^{-1}$)[b] | |
|---|---|---|---|---|---|---|---|---|
| | calcd | exptl | top | bridge | fcc | hcp | calcd | exptl |
| H | top | top[c] | **−2.73 [−2.62]** | −2.58 [−2.43] | −2.60 [−2.45] | −2.50 [−2.44] | 2155 | 2030[c] |
| O | fcc | fcc[d] | −3.46 [−3.04] | −4.02 [−3.51] | **−4.57 [−4.00]** | −4.32 [−3.75] | 485[e] | 550[f,g,h] |
| N | fcc/hcp | | −3.48 [−3.26] | −4.25 [−3.90] | **−4.80 [−4.40]** | **−4.80 [−4.40]** | 516 (fcc), 546 (hcp) | |
| S | fcc | fcc[i] | −3.24 [−2.86] | −4.53 [−4.10] | **−5.11 [−4.67]** | −5.07 [−4.63] | 362 (fcc), 372 (hcp) | |
| C | hcp | | −5.30 [−5.02] | −6.21 [−5.82] | −6.54 [−6.13] | **−6.71 [−6.29]** | 479 | |

[a] The reference zero corresponds to gas-phase atoms at infinite separation from the iridium slab. The most favorable site for each adsorbate and the corresponding binding energies are indicated in bold. [b] Evaluated at preferred site. [c] Reference 18. [d] Reference 10. [e] Also calculated by ref 47. [f] Reference 6. [g] Reference 15. [h] Reference 51. [i] Reference 17.

**TABLE 2: Vertical Distance between the Adsorbate and the Plane of Three Metal Atoms Defining the Corresponding Site on Relaxed Surfaces ($d_{A-Ir}$), Intraadsorbate ($d_{A-B}$) Bond Lengths, Displacement of the Plane of Three Metal Atoms Defining the Corresponding Sites with Respect to the Clean, Relaxed Surface ($\Delta_{z-Ir}$), and Metal−Metal Bond Length ($d_{Ir-Ir}$) on the Relaxed Surface[a]**

| adsorbates | $d_{A-Ir}$ (Å) | $\Delta_{z-Ir}$ (Å) | $d_{Ir-Ir}$ (Å) | $d_{A-B}$ (Å) |
|---|---|---|---|---|
| H (top) | 1.59 | 0.09 | ... | ... |
| O (fcc) | 1.23 | 0.07 | 2.83 | ... |
| N (fcc) | 1.09 | 0.11 | 2.83 | ... |
| N (hcp) | 1.11 | 0.09 | 2.81 | ... |
| S (fcc) | 1.68 | 0.07 | 2.79 | ... |
| C (hcp) | 1.07 | 0.09 | 2.82 | ... |
| $N_2$ (top) | 1.90 | 0.20 | ... | 1.14 |
| $NH_3$ (top) | 2.16 | 0.07 | ... | 1.03 |
| NO (top) | 1.75 | 0.30 | ... | 1.18 |
| $CH_3$ (top) | 2.11 | 0.15 | ... | 1.10 |
| CO (top) | 1.83 | 0.24 | ... | 1.17 |
| OH (tilted top)[b] | 2.09 | −0.01 | ... | 0.99 |
| NOH (bent fcc)[c] | 1.16 | 0.10 | 2.84 | 1.41(N−O), 0.99(O−H) |

[a] Only the most favorable site is analyzed. A schematic representation is given in Figure 3. $d_{Ir-Ir}$ on a clean relaxed surface = 2.73 Å. [b] 20.1° angle with the surface. [c] NO perpendicular to surface, OH 16.2° to the surface plane.

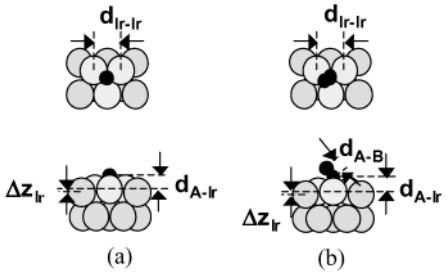


**Figure 3.** Schematic representation of top and side views of various adsorbates on 3-fold sites of Ir(111): (a) atomic adsorbates and (b) molecular and radical adsorbates. Geometrical parameters shown are listed in Table 2.

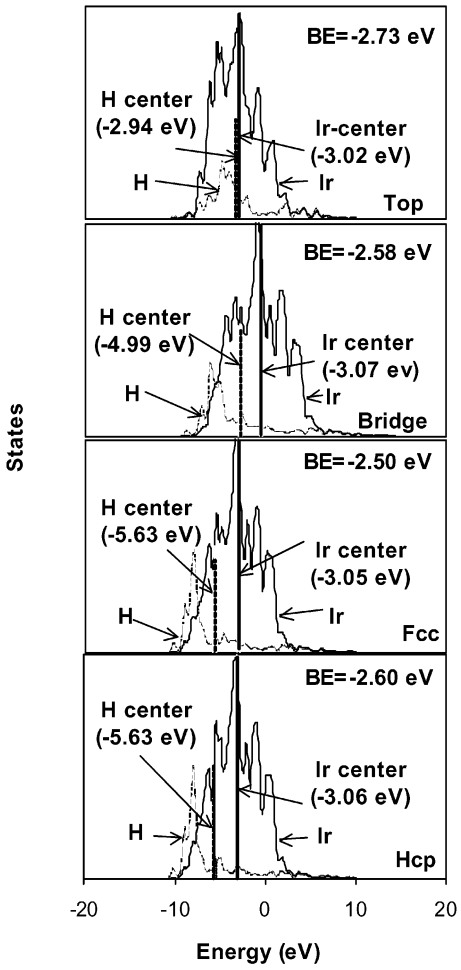


**Figure 4.** Density of state plots for hydrogen (s-bands) and Ir-surface atoms (d-bands) in the (from top to bottom) top, bridge, fcc, and hcp configurations.

binding energy of −2.73 [−2.62] eV (Table 1). The most energetically favorable configuration is that with the hydrogen atop an iridium atom (Figure 1). The geometric parameters for this configuration are given in Table 2. A Redhead analysis of TPD data at 0.18 ML,[18] assuming a preexponential factor of $10^{13}$, gives an experimental estimate for the associative desorption energy of $H_2$ of 0.73 eV, compared to a value of 0.89 eV calculated with our data. Figure 3 shows a schematic representation of the corresponding structural parameters. The determination of a favorable atop configuration is consistent with HREELS experiments[18] at a coverage of 0.44 ML on Ir(111). Furthermore, the calculated perpendicular H−metal stretch at 2155 cm$^{-1}$ (Table 1) is in good agreement with the experimental stretch at 2030 cm$^{-1}$.[18] The preference of hydrogen for atop sites can be explained by comparing the hydrogen s-bands with the iridium d-bands for various adsorption configurations; the atop configuration gives the best orbital overlap between these bands (Figure 4). The estimated diffusion barrier for hydrogen is 0.13 [0.17] eV (Table 3, Figure 2). The effect of surface relaxation on the hydrogen binding energy was found to be small (0.004 [0.02] eV stabilization), and a small upward displacement of the H-coordinated iridium atom (0.09 Å, Table 2) was observed.

The next least strongly bound atom studied was *oxygen*. The preferred binding site was fcc with a binding energy of −4.57 [−4.00] eV (Table 1). Chan et al. also found with LEED experiments that the preferred site is fcc for oxygen atoms

**TABLE 3: Lower Estimates for the Diffusion Barriers of Atomic Species on Ir(111) Based on Thermochemical Data[a]**

| adsorbate | diffusion barrier (eV) PW91 | RPBE |
|---|---|---|
| H[b] | 0.13 | 0.17 |
| O | 0.55 | 0.49 |
| N | 0.55 | 0.50 |
| S | 0.58 | 0.57 |
| C | 0.49 | 0.47 |
| $NH_3$[c] | 0.71 | 0.51 |
| NO | 0.01 | 0.08 |
| $CH_3$ | 0.38 | 0.48 |
| CO | 0.43 | 0.49 |
| OH (tilted) | 0.02 | 0.10 |
| NOH (tilted)[d] | 0.53 | 0.44 |

[a] Unless otherwise stated, atomic diffusion is threefold-bridge-threefold, and molecular diffusion is top-bridge-top. [b] Top-fcc-top. [c] Top-hcp-top. [d] Fcc-top-fcc.

forming a (2×2) superstructure.[10] In addition, the fcc preference for adsorbed oxygen has been observed on the (111) facets of several other fcc metals.[47−50] We estimated the perpendicular O−metal stretch to be 485 $cm^{-1}$ (Table 1), in good agreement with a previous DFT study.[47] Experimentally, the loss peak for oxygen determined by EELS over a wide range of temperatures is 550 $cm^{-1}$; this peak was attributed to a single chemisorbed state for atomic oxygen on Ir(111).[6,15,51] We estimate a diffusion barrier for oxygen on Ir(111) of 0.55 [0.49] eV (Table 3). The effect of surface relaxation on the binding energy was again small (0.03 [0.04] eV stabilization), but it did result in a modest increase in the Ir−Ir distance of the nearest neighbor Ir atoms (0.10 Å) surrounding the oxygen atom (Table 2).

For *nitrogen*, there was found to be a degeneracy of most favorable binding sites (fcc and hcp) with binding energies of −4.80 [−4.40] eV (Table 1). The estimated diffusion barrier was 0.55 [0.50] eV (Table 3). Surface relaxation yielded a modest stabilization (0.07 [0.08] eV change in binding energy). Interestingly, a nitrogen adatom in the fcc position was found to displace Ir atoms to a greater extent then the degenerate hcp configuration (Table 2); the Ir−Ir distance was 2.83 Å for fcc adsorption and 2.81 Å for hcp adsorption (compared to 2.73 Å for the clean, relaxed surface), and there were upward shifts of the nearest neighbor Ir atoms of 0.11 Å for fcc adsorption and 0.09 Å for hcp adsorption (compared to the clean, relaxed surface). This increased surface deformation resulted in greater destabilization of the surface, as seen in the increased deformation energy (Table 7). This energy, defined as the energy of the relaxed surface (with the adsorbate removed) minus the energy of the relaxed clean surface, represents the elastic energy required to deform the surface to accommodate the adsorbate. Since the adsorption energies at the fcc and hcp sites are equal, the higher deformation energy at the fcc site must be compensated for by a greater electronic interaction of nitrogen with the surface at fcc sites. The perpendicular N−metal stretch was calculated to be 516 and 546 $cm^{-1}$ for the fcc and hcp configurations, respectively (Table 1). We were unable to find any experimental vibrational data for nitrogen on Ir(111) for comparison.

Strong binding to Ir(111) is exhibited by *sulfur*. The preferred binding site was determined to be fcc with a binding energy of −5.11 [−4.67] eV (Table 1). This preference for adsorption at the fcc location is consistent with LEED experiments at 1/3 ML.[17] These experiments also determined the Ir−S bond length to be 2.28 Å, in good agreement with the value of 2.32 Å calculated here. The hcp site was almost degenerate, however, with an energy only 0.04 [0.04] eV greater than the energy of the fcc configuration. The estimated diffusion barrier was 0.58 [0.57] eV (Table 3). For adsorption in the fcc site, the change in binding energy due to surface relaxation is small. There was an increase in the Ir−Ir spacing (0.06 Å) and a small upward shift of the sulfur-coordinated iridium atoms (0.07 Å) (Table 2). The vibrational modes for the S−metal stretch in the fcc and hcp sites were calculated as 362 and 372 $cm^{-1}$, respectively (Table 1). No experimental vibrational data for sulfur on Ir(111) were available for comparison.

The most strongly bound atom studied on Ir(111) was *carbon*. The preferred binding site is hcp with a binding energy of −6.71 [−6.29] eV (Table 1). The barrier for diffusion of C is estimated to be 0.49 [0.47] eV (Table 3). The stabilization due to surface relaxation is significant (0.10 [0.12] eV increase in binding energy). In the hcp configuration, the Ir−Ir distance increases by 0.09 Å from the corresponding distance on the clean, relaxed surface. This large movement is reflected in the iridium slab deformation energy of 0.22 [0.19] eV (Table 7). The large deformation energy suggests that the strength of the electronic interaction of C with the surface should be even greater than the binding energy given above. The vibrational frequency of carbon in the hcp site is calculated to be 479 $cm^{-1}$ (Table 1). We were unable to find any experimental vibrational data for carbon on Ir(111).

**General Binding Trends for Atomic Adsorbates.** A preference for 3-fold sites is observed for all the atomic adsorbates studied with the exception of hydrogen. This suggests that gas-phase bonding trends are not always followed by atomic adsorbates on the Ir(111) surface. For instance, oxygen and sulfur bind to at most two atoms in the gas phase, yet both atoms preferentially adsorb in 3-fold sites on the Ir(111) surface. However, the other atomic adsorbates follow typical gas-phase coordination trends. Nitrogen typically forms three bonds in the gas phase, but it also forms bonds with four atoms in compounds such as ammonium. These facts are consistent with the degenerate preference for either the fcc or hcp sites on the Ir(111) surface. Carbon typically forms tetravalent coordinated compounds in the gas phase, consistent with its preference for hcp sites on Ir(111). Hydrogen typically forms one bond, consistent with its preference for adsorption at top Ir(111) sites.

Table 2 shows a general trend in the geometry changes of top-layer iridium atoms due to adsorption in 3-fold sites. An increase in $d_{Ir-Ir}$ is observed in all cases. Thus, atomic adsorption in the 3-fold sites of Ir(111) causes a radial *outward* shift of the iridium surface atoms.

**Adsorption of Molecules and Radicals.** The least strongly bound of the molecular adsorbates is $N_2$. The favored configuration is perpendicular to the surface, atop an iridium atom, with a binding energy of −0.54 [−0.21] eV (Table 4). The only significantly stable $N_2$ molecular state is at the top site, so estimation of a diffusion barrier for $N_2$ on Ir(111) is meaningless. The molecular N−N stretch is 2223 $cm^{-1}$ (Table 5). This compares well with EELS experiments which determined the stretch to be ca. 2210 $cm^{-1}$.[6] The effect of surface relaxation was significant; a 0.13 [0.15] eV increase in binding energy magnitude was found, and a significant upward shift of 0.20 Å of the iridium atom coordinated to the $N_2$ molecule (Table 2, Figure 5) was observed.

The favored binding site for *ammonia* is on top of an iridium atom, with the nitrogen bonding to iridium and the hydrogen atoms in the direction of bridge sites. The binding energy of this configuration is −0.84 [−0.47] eV (Table 4). Configurations with the hydrogen atoms in the direction of 3-fold sites had minimal differences in the binding energy (less than 0.01 eV).

**TABLE 4: Calculated Binding Energies of Molecular and Radical Adsorbates on a Relaxed Ir(111) Surface at 0.25 ML Coverage[a]**

| | preferred site | | calculated binding energy (eV) PW91 [RPBE] | | | |
|---|---|---|---|---|---|---|
| | calcd | exptl | top | bridge | fcc | hcp |
| $N_2$ | top | | **−0.54 [−0.21]** | | −0.02 [0.06] | −0.04 [0.03] |
| $NH_3$ | top | fcc/hcp[b] | **−0.84 [−0.47]** | −0.08 [0.10] | −0.13 [0.05] | −0.13 [0.04] |
| NO | top | top[c] | **−1.81 [−1.38]** | −1.80 [−1.30] | −1.68 [−1.14] | −1.72 [−1.18] |
| $CH_3$ | top | | **−1.88 [−1.55]** | −1.50 [−1.07] | −1.38 [−0.91] | −1.31 [−0.84] |
| CO | top | top[d] | **−2.13 [−1.78]** | −1.70 [−1.29] | −1.56 [−1.13] | −1.69 [−1.25] |
| OH | top | | **−2.52[e,f] [−2.05]**[e,f] | −2.50[e] [−1.96][e] | −2.27 [−1.70] | −2.10 [−1.54] |
| NOH (bent)[g] | fcc | | −3.82 [−3.22] | −3.57 [−2.94] | **−4.35[h] [−3.66]**[h] | −4.20 [−3.52] |

[a] All configurations are perpendicular to the surface, unless indicated otherwise. Preferred sites are shown in bold. The reference zero corresponds to gas-phase atoms at infinite separation from the iridium slab. [b] Reference 28; 1 ML coverage. [c] Suggested by ref 6 (see text). [d] Reference 22. [e] Tilted configuration. [f] 20.1° to the surface. [g] Reference gas-phase energy taken as NO(g) + H(g). [h] NO perpendicular to surface, OH 16.2° to the surface plane.

**TABLE 5: Intramolecular (IM) Stretch and Adsorbate−Surface (AM) Stretch Vibrational Frequencies for Diatomic Molecular and Radical Adsorbates in Preferred Sites[a]**

| | $\nu$ ($cm^{-1}$) | | |
|---|---|---|---|
| | calcd | | exptl |
| adsorbate | IM | AM | IM |
| $N_2$ (top) | 2223 | 403 | 2210[b] |
| NO (top) | 1923 | 525 | 1860[c] |
| NO (br) | 1669 | 364 | |
| NO (hcp) | 1536 | 337 | 1550[d] |
| CO (top) | 2114 | 498 | 2065[e] |
| OH (tilted) (top) | 3756 | 524[f] | |
| OH (tilted) (br) | 3668 | 408[g] | |

[a] Experimental data are included where available. [b] Reference 6. [c] Reference 20. [d] Suggested by comparison with results from ref 20 (see text). [e] Reference 22. [f] A strong OH bend is also found at 892 $cm^{-1}$. [g] Strong OH bends are also found at 715 and 726 $cm^{-1}$.

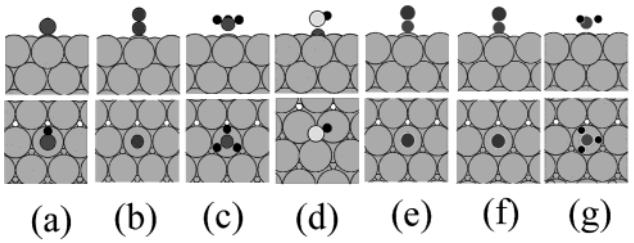


**Figure 5.** Preferred binding modes for molecular and radical adsorbates on Ir(111): (a) OH (tilted) top, (b) $N_2$ top, (c) $CH_3$ top, (d) NOH (bent) fcc, (e) CO top, (f) NO top, and (g) $NH_3$ top.

A diffusion barrier (top-hcp-top) of 0.71 [0.51] eV is estimated (Table 3, Figure 2). Angle-resolved photoemission measurements of ammonia adsorption on Ir(111) showed the favored position to be fcc.[28] However, that study was conducted at a saturated surface coverage. The difference in coverages between that study and ours (0.25 ML) could have led to the observation of different site preferences. Also, the experimental work function change ($\Delta\phi$) was found to be approximately −2.5 eV,[28] compared to −2.9 eV calculated in the present study. This difference might, again, be caused by the different coverages used in the two studies. The effect of surface relaxation was determined to be minimal. Geometric parameters for adsorbed ammonia are given in Table 2. Selected calculated vibrations for ammonia are a N−H symmetric stretch at 3333 $cm^{-1}$, a N−H antisymmetric stretch at 3427 $cm^{-1}$, an adsorbate−surface stretch at 264 $cm^{-1}$, and a $NH_3$ deformation at 960 $cm^{-1}$ (Table 6).

**TABLE 6: Selected Vibrational Frequencies for Polyatomic Molecular and Radical Adsorbates in Preferred Sites**

| | $\nu$ ($cm^{-1}$) | | |
|---|---|---|---|
| mode | $CH_3$ (top) | $NH_3$ (top) | NOH (bent fcc) |
| intramolecular stretch | 2990[a] | 3333[a] | 3694[b] |
| | 3087[c] | 3427[c] | 816[d] |
| adsorbate−surface stretch | 491 | 264 | 287 |
| scissor | 1390 | 1506 | 1272 |
| bend | 753 | 628 | 527/529 |
| deformation | 1192 | 960 | |

[a] Symmetric. [b] O−H. [c] Antisymmetric. [d] N−O.

The favored binding site for NO is atop with a binding energy of −1.81 [−1.38] eV (Table 4), but the bridge and hcp sites are quasi-degenerate with the top site. A top site preference is also suggested by TPD and EELS studies.[6] A diffusion barrier (top-bridge-top) of 0.01 [0.08] eV is estimated (Table 3). EELS experiments at <0.1 ML show the N−O stretch to be at 1860 $cm^{-1}$,[20] compared to our calculated value of 1923 $cm^{-1}$ (Table 5). Also, in the same experimental study, a mode was observed at 1550 $cm^{-1}$ at temperatures less than 400 K, which could correspond to an hcp bonded NO molecule for which we calculated the frequency to be 1536 $cm^{-1}$. Surface relaxation had a significant effect on NO binding in fcc sites (0.25 eV stabilization), as is seen by the large vertical displacement of the adsorbate-coordinated iridium atom of 0.30 Å (Table 2) and the large deformation energy of 0.40 eV (Table 7). Interestingly, the deformation energy for NO at top sites is much greater than that at bridge sites (0.40 eV vs 0.24 eV, Table 7). Since the binding energies for these two configurations are essentially equal, the higher deformation energy at the top site must be compensated for by a greater electronic interaction of NO with the surface at top sites. Finally, NO showed a site preference change from the static surface (hcp) to the relaxed surface (top/bridge).

The *methyl radical* also favors the atop configuration, binding through the carbon atom with the hydrogen atoms pointed toward the neighboring fcc sites (Figure 5). This atop site preference is in agreement with other slab DFT studies of the methyl radical.[27] A binding energy of −1.88 [−1.55] eV is calculated (Table 4), and a diffusion barrier of 0.38 [0.48] eV (Table 3) is estimated. Configurations with the hydrogen atoms in the direction of 3-fold sites had minimal differences in binding energy (<0.01 eV). The effects of surface relaxation were a 0.14 [0.13] eV increase in binding energy magnitude and a 0.15 Å upward shift of the $CH_3$-coordinated iridium atom (Table 2). Selected vibrations for the methyl radical were a C−H symmetric stretch at 2990 $cm^{-1}$, a C−H antisymmetric stretch at

**TABLE 7: Energy Increase (Deformation Energy) of Relaxed Surface with Adsorbates Removed Relative to Relaxed Clean Surface[a]**

| | | $\Delta E$ (eV) | |
|---|---|---|---|
| | | PW91 | RPBE |
| H | top | 0.04 | 0.04 |
| C | hcp | 0.22 | 0.19 |
| N | fcc | 0.26 | 0.23 |
| N | hcp | 0.20 | 0.17 |
| O | fcc | 0.17 | 0.15 |
| S | fcc | 0.09 | 0.07 |
| S | hcp | 0.12 | 0.10 |
| $N_2$ | top | 0.20 | 0.18 |
| $NH_3$ | top | 0.03 | 0.02 |
| NO | top | 0.40 | 0.37 |
| NO | br | 0.24 | 0.22 |
| $CH_3$ | top | 0.12 | 0.11 |
| CO | top | 0.27 | 0.25 |
| OH (tilted) | top | 0.07 | 0.07 |
| NOH (bent) | fcc | 0.25 | 0.22 |

[a] $\Delta E$ = *E*(relaxed surface with adsorbate removed) − *E*(clean surface). Multiple sites are reported for a given species if these sites are very close to each other energetically.

3087 $cm^{-1}$, an adsorbate−surface stretch at 491 $cm^{-1}$, and a $CH_3$ deformation at 1192 $cm^{-1}$.

CO is another diatomic molecule that prefers top sites, bound through the carbon atom and oriented perpendicular to the surface (Figure 5). A binding energy of −2.13 [−1.78] eV is calculated (Table 4), and a diffusion barrier of 0.43 [0.49] eV (top-bridge-top) is estimated (Table 3). In LEED experiments,[23] the isosteric heat of adsorption for surface coverages of less than 0.3 ML was found to be in excess of 1.96 eV, close to our reported binding energy. Surface relaxation causes an upshift of the CO-coordinated iridium atom of 0.24 Å (Table 2) and a 0.16 [0.20] eV increase in the magnitude of the binding energy. IRAS data agree with the preference for top sites at surface coverages of 0.25 ML.[22] Finally, the calculated C−O stretch (Table 5), 2114 $cm^{-1}$, agrees well with an experimental value of approximately 2065 $cm^{-1}$.[22]

Two structural states were investigated for OH, one perpendicular to the surface and the other tilted toward the surface. Both states were bound to the surface through oxygen. The perpendicular state was found to prefer fcc sites with a binding energy of −2.27 [−1.70] eV. The tilted configuration was determined to be even more stable (binding energy of −2.52 [−2.05] eV, Table 4) and preferred top sites; the hydrogen points toward neighboring fcc sites, making a 20.1° angle with the surface. The diffusion barrier for the tilted OH is estimated to be very small at 0.02 [0.10] eV (top-bridge-top). Interestingly, the hydroxyl radical induced a *downward shift* of the coordinated iridium atom by 0.01 Å (Table 2). OH was the only multiatom adsorbate to exhibit this behavior. Energetically, the effect of surface relaxation was small. The O−H intramolecular and adsorbate−surface stretches were calculated as 3756 and 524 $cm^{-1}$, respectively.

Three structural states were investigated for the NOH radical species; (1) perpendicular to the surface and bound through N, (2) bound to the surface through N with O−H tilted toward the surface, and (3) bound to the surface through N (N on top of an Ir atom, O close to an adjacent Ir atom, and H above N). The most stable perpendicular configuration (1) was ca. 1.7 eV less stable than the most stable bent configuration (2). The most stable configuration for the state bound through N to the surface (3) was ca. 0.15 eV less stable than the most stable bent state (2). The overall most stable configuration was with the nitrogen in the fcc position, the oxygen directly above it, and the hydrogen pointing toward a top location at an angle of 16.2° above the surface plane (configuration (2), Figure 5). The binding energy for this state was −4.35 [−3.66] eV. The diffusion barrier for NOH in this configuration was estimated to be ca. 0.53 [0.44] eV (fcc-top-fcc, Table 3). The effect of surface relaxation was a 0.06 [0.06] eV increase in binding energy and an increase in the Ir−Ir distance of 0.11 Å from the corresponding equilibrium distance (Table 2). An O−H stretch was found at 3694 $cm^{-1}$, an O−N stretch was found at 816 $cm^{-1}$, and a N−Ir stretch was found at 287 $cm^{-1}$.

**General Binding Trends for Molecular and Radical Adsorbates.** Our results show that all radical and molecular adsorbates, except for NOH and the degenerate bridge-bonded state of NO, are preferentially adsorbed in the top sites. This can be explained by analogy to gas-phase bonding, as suggested by Michaelides et. al on Pt(111).[52] $N_2$, $NH_3$, and CO are stable in the gas phase, so the lowest possible coordination is expected in the adsorbed state. Carbon typically forms tetravalent compounds, so the atop configuration may be expected for the methyl radical. Nitrogen is trivalent, so again, an on-top configuration is expected for NO. Likewise, since oxygen is divalent, an atop adsorbed state is reasonable for OH.

When the surface is allowed to relax, similar trends as seen in atomic adsorption are observed. For on-top adsorption, an upshift in the coordinated Ir atom is observed, with the exception of the hydroxyl radical. Also, adsorption in 3-fold sites (NOH, fcc) resulted in an increase in Ir−Ir spacing from the corresponding clean slab spacing. Table 2 summarizes these results.

For all the adsorbates investigated here, a large decrease in binding energy magnitude is observed by going from PW91 to RPBE (of the order of tenths of an eV, Tables 1 and 4). These downward shifts are approximately constant for different configurations of a given adsorbate. Thus, there are only small changes in the estimated diffusion barriers (less than 0.1 eV) (Table 3) between the two functionals. The differences between RPBE and PW91 may be a result of the different ways the high electron density gradients in the gas-phase species are treated by the two functionals. Finally, based on the calculated binding energies, molecular and radical adsorbates should diffuse from top sites to bridge sites to top sites, except for NOH, which should diffuse from 3-fold sites to 3-fold sites via top sites. $NH_3$ might diffuse between top sites via either 3-fold or bridge sites.

## 4. Thermochemistry of CO, NO, NOH, $N_2$, $NH_3$, and $CH_3$ Dissociation

The calculated binding energies and gas-phase total energies of several atomic and molecular species were used to construct eight simple thermochemical reaction pathways. Parts a and b of Figure 6 provide the thermochemistry of CO, NO, NOH, $N_2$, $NH_3$, and $CH_3$ decomposition on Ir(111) based on the PW91 and RPBE functionals, respectively.

For CO dissociation, there is a −0.32 [+0.29] eV change in energy due to adsorption followed by decomposition of CO. Thus, thermodynamically, PW91 predicts dissociation and RPBE predicts desorption as energetically more probable events for adsorbed CO. Experiments show that at $T > 650$ K and $P > 10^{-6}$ Torr, dissociation occurs.[23]

The second thermochemical pathway we investigated was the adsorption and decomposition of NO (Figure 6). The thermochemistry of this reaction is of particular interest for the improvement of the automobile catalytic converter.[6] The energy change due to dissociative adsorption of NO on Ir(111) is −2.63

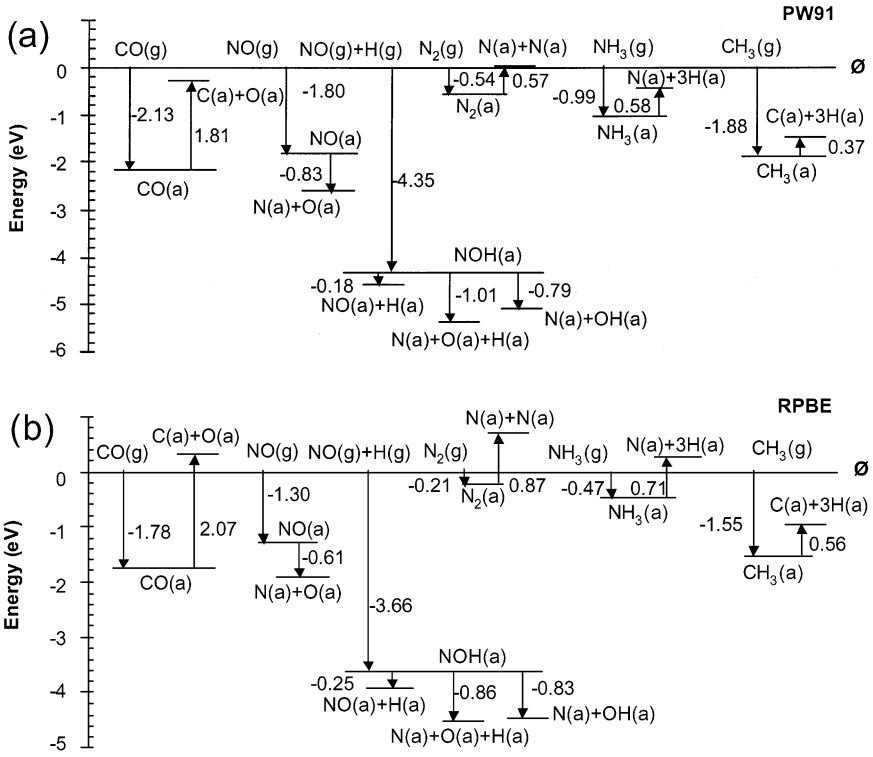


**Figure 6.** Thermochemistry of molecular decomposition on the Ir(111) surface. Reference zero corresponds to gas-phase molecules/radicals and a Ir(111) slab at infinite separation. Energetics calculated with the (a) PW91 and (b) RPBE functionals.

[−1.91] eV. Also, the dissociation of adsorbed NO on Ir(111) is exothermic and thermodynamically favorable (−0.83 [−0.61] eV). These results imply that adsorbed NO is expected to dissociate rather than desorb. Experiments show that terminally bonded NO dissociates totally upon heating.[6,53]

The dissociation of the NOH radical was also investigated (Figure 6) for three different pathways. This process is exothermic. The most favorable mechanism is that which results in complete dissociation of adsorbed NOH to its atomic constituents with a −1.01 [−0.86] eV net energy change. The second thermodynamically best decomposition yields N(a) + OH(a), and the least favored decomposition yields NO(a) + H(a).

The dissociative adsorption of $N_2$ has a net energy cost of 0.03 [0.66] eV. Thus, $N_2$ desorption is thermodynamically preferable to dissociation on Ir(111). This is in agreement with TPD and LEED experiments[6] which determined that no atomic nitrogen was produced upon heating of adsorbed $N_2$.

The next thermochemical pathway investigated was that of ammonia dissociative adsorption. As shown in Figure 6, this process is thermodynamically favorable according to the PW91 functional and slightly endothermic according to the RPBE functional.

The last thermochemical pathway investigated was the adsorption and complete decomposition of the methyl radical on Ir(111). The energy change of this process is −1.51 [−0.99] eV. Figure 6 also shows that the decomposition is thermodynamically favorable to desorption. This process is of industrial interest in that Ir and Ir−alloy catalysts are used in reactions that require the activation of C−H bonds.[1]

## 5. Conclusions

The chemisorption of atomic (H, O, N, S, C), molecular ($N_2$, CO, NO, $NH_3$), and radical ($CH_3$, OH, NOH) species on Ir(111) has been systematically studied. Self-consistent, periodic, density functional theory (DFT-GGA) calculations, using PW91 and RPBE functionals, have been used to determine preferred binding sites, chemisorbed structures, binding energies, vibrational frequencies, and the effect of surface relaxation for the above species at 0.25 ML surface coverage. The following order in binding energies from least to most strongly bound species was determined: $N_2$ < $NH_3$ < NO < $CH_3$ < CO < OH < H < NOH < O < N < S < C. This trend was observed with both PW91 and RPBE functionals. A preference for 3-fold sites for the atomic adsorbates was observed, with the exception of atomic H; this species preferred top sites. Molecular species showed a preference for top sites with the exception of NOH, which preferred fcc sites. Surface relaxation had only a small effect on energetics in most cases. Calculated vibrational frequencies compared well with experiments where data were available. Finally, the thermochemistry of CO, NO, NOH, $N_2$, $NH_3$, and $CH_3$ decomposition on Ir(111) was examined.

**Acknowledgment.** W.P.K. acknowledges partial financial support from a UW-Madison Hilldale fellowship for undergraduate research. J.G. acknowledges partial financial support from a National Science Foundation predoctoral fellowship. M.M. acknowledges financial support from an NSF-CAREER Award (CTS-0134561) and a 3M Faculty award. We thank BP-Amoco for an equipment grant. This research used resources of the National Energy Research Scientific Computing Center, which is supported by the Office of Science of the U.S. Department of Energy under Contract No. DE-AC03-76SF00098. All authors acknowledge partial support from NSF cooperative agreement ACI-9619020 through computing resources provided by the National Partnership for Advanced Computational Infrastructure (NPACI).

## References and Notes

(1) Johnson, D. F.; Weinberg, W. H. *Science* **1993**, *261*, 71.

(2) Sinfelt, J. H. *Bimetallic Catalysts*: *Discoveries, Concepts, and Applications*; Wiley: New York, 1983.

(3) Seets, D. C.; Wheeler, M. C.; Mullins, C. B. *Chem. Phys. Lett.* **1997**, *266*, 431.
(4) Seets, D. C.; Reeves, C. T.; Ferguson, B. A.; Wheeler, M. C.; Mullins, C. B. *J. Chem. Phys.* **1997**, *107*, 10229.
(5) Choudhary, T. V.; Sivadinarayana, C.; Goodman, D. W. *Chem. Eng. J.* **2003**, *93*, 69.
(6) Cornish, J. C. L.; Avery, N. R. *Surf. Sci*. **1990**, *235*, 209.
(7) Wögerbauer, C.; Maciejewski, M.; Baiker, A. *J. Appl. Catal. B* **2001**, *34*, 11.
(8) Haynes, A.; Pearson, J. M.; Vickers, P. W.; Charmant, J. P. H.; Maitlis, P. M. *Inorg. Chim. Acta* **1998**, *270*, 382.
(9) Marales-Morales, D.; Lee, D. W.; Wang, Z. H.; Jensen, C. M. *Organometallics* **2001**, *20*, 1144.
(10) Chan, C. M.; Weinberg, W. H. *J. Chem. Phys.* **1979**, *71*, 2788.
(11) Hagen, D. I.; Nieuwenhuys, B. E.; Rovida, G.; Somorjai, G. A. *Surf. Sci* **1976**, *57*, 632.
(12) Tucker, C. W. *J. Appl. Phys.* **1964**, *35*, 1897.
(13) Küppers, J.; Plagge, A. *J. Vac. Sci. Technol.* **1976**, *13*, 259.
(14) Zhdan, P. A.; Boreskov, G. K.; Boronin, A. I.; Egelhoff, W. F., Jr.; Weinberg, W. H. *Surf. Sci* **1976**, *61*, 25.
(15) Marinova, T. S.; Kostov, K. L. *Surf. Sci.* **1987**, *185*, 203.
(16) Nieuwenhuys, B. E.; Somorjai, G. A. *Surf. Sci.* **1978**, *72*, 8.
(17) Chan, C. M.; Weinberg, W. H. *J. Chem. Phys.* **1979**, *71*, 3988.
(18) Hagedorn, C. J.; Weiss, M. J.; Weinberg, W. H. *Phys. Rev. B* **1999**, *60*, R14 016.
(19) Schick, M.; Lauterbach, J.; Weinberg, W. H. *Surf. Sci.* **1996**, *14*, 1511.
(20) Davis, J. E.; Karseboom, S. G.; Nolan, P. D.; Mullins, C. B. *J. Chem. Phys.* **1996**, *105*, 8362.
(21) Koper, M. T. M.; van Santen, R. A.; Wasileski, S. A.; Weaver, M. J. *J. Chem. Phys.* **2000**, *113*, 4392.
(22) Lauterbach, J.; Boyle, R. W.; Schick, M.; Mitchell, W. J.; Meng, B.; Weinberg, W. H. *Surf. Sci*. **1996**, *350*, 32.
(23) Comrie, C. M.; Weinberg, W. H. *J. Chem. Phys.* **1976**, *64*, 250.
(24) Zhdan, P. A.; Boreskov, G. K.; Baronin, A. I.; Egelhoff, W. F., Jr.; Weinberg, W. H. *Chem. Phys. Lett.* **1976**, *44*, 528.
(25) Sushchikh, M.; Lauterbach, J.; Weinberg, W. H. *J. Vac. Sci. Technol. A* **1997**, *15*, 1630.
(26) Burghaus, U.; Ding, J.; Weinberg, W. H. *Surf. Sci* **1997**, *384*, L869.
(27) Henkelman, G.; Jónsson, H. *Phys. Rev. Lett.* **2001**, *86*, 664.
(28) Purtell, R. J.; Merrill, R. P.; Seabury, C. W.; Rhodin, T. N. *Phys. Rev. Lett.* **1980**, *44*, 1279.
(29) Santra, A. K.; Min, B. K.; Yi, C. W.; Luo, K.; Choudhary, T. V.; Goodman, D. W. *J. Phys. Chem. B* **2002**, *106*, 340.
(30) Carabineiro, S. A. C.; Nieuwenhuys, B. E. *Surf. Sci.* **2002**, *505*, 163.
(31) Burghaus, U.; Ding, J.; Weinberg, W. H. *J. Vac. Sci. Technol. A* **1998**, *16*, 1010.
(32) Sushchikh, M.; Lauterbach, J.; Weinberg, W. H. *Surf. Sci.* **1997**, *393*, 135.
(33) Weinberg, W. H.; Comrie, C. M.; Lambert, R. M. *J. Catal.* **1976**, *41*, 489.
(34) Liu, Z.-P.; Hu, P. *J. Chem. Phys.* **2001**, *114*, 8244.
(35) Personal communication from W. H. Weinberg.
(36) Greeley, J. G.; Nørskov, J. K.; Mavrikakis, M. *Annu. Rev. Phys. Chem.* **2002**, *53*, 319.
(37) Mavrikakis, M.; Rempel, J.; Greeley, J.; Hansen, L. B.; Nørskov, J. K. *J. Chem. Phys.* **2002**, *117*, 6737.
(38) Hammer, B.; Hansen, L. B.; Nørskov, J. K. *Phys. Rev. B* **1999**, *59*, 7413.
(39) Neugebauer, J.; Scheffler, M. *Phys. Rev. B* **1992**, *46*, 16067.
(40) Vanderbilt, D. *Phys. Rev. B* **1990**, *41*, 7892.
(41) Perdew, J. P.; Chevary, J. A.; Vosko, S. H.; Jackson, K. A.; Pederson, M. R.; Singh, D. J.; Fiolhais, C. *Phys. Rev. B* **1992**, *46*, 6671.
(42) White, J. A.; Bird, D. M. *Phys. Rev. B* **1994**, *50*, 4754.
(43) Kresse, G.; Furthmuller, J. *Comput. Mater. Sci.* **1996**, *6*, 15.
(44) Donohue, J. *The Structure of the Elements*; Wiley: New York, 1974; p 218.
(45) Greeley, J.; Mavrikakis, M. *Surf. Sci* **2003**, *540*, 215.
(46) Chase, M. W., Jr. *NIST-JANAF Thermochemical Tables*, 4th ed.; American Chemical Society: Washington, DC, 1998; Monograph 9.
(47) Xu, Y.; Mavrikakis, M. *J. Chem. Phys.* **2002**, *116*, 10846.
(48) Eichler, A.; Mittendorfer, F.; Hafner, J. *Phys. Rev. B* **2000**, *62*, 4744.
(49) Xu, Y.; Mavrikakis, M. *J. Phys. Chem. B.* **2003**, *107*, 9298.
(50) Xu, Y.; Mavrikakis, M. *Surf. Sci.* **2001**, *494*, 131.
(51) Davis, J. E.; Nolan, P. D.; Karseboom, S. G.; Mullins, C. B. *J. Chem. Phys.* **1997**, *107*, 943.
(52) Michaelides, A.; Hu, P. *J. Am. Chem. Soc.* **2000**, *122*, 9866.
(53) Davis, J. E.; Karseboom, S. G.; Nolan, P. D.; Mullins, C. B. *J. Vac. Sci. Technol. A* **1996**, *45*, 1598.